


Observation of strong and anisotropic nonlinear optical effects through polarization-resolved optical spectroscopy in the type-II Weyl semimetal T_d -WTe₂

Elizabeth Druke ^{1,*}, Junjie Yang,² and Liuyan Zhao^{1,†}

¹*Department of Physics, University of Michigan, 450 Church Street, Ann Arbor, Michigan 48109, USA*

²*Department of Physics, New Jersey Institute of Technology, University Heights Tiernan Hall Room 463, University Heights, Newark, New Jersey 07102, USA*



(Received 3 November 2020; accepted 27 July 2021; published 9 August 2021)

The unique bulk crossing points in the band structure of topological Weyl semimetals have been shown to enhance nonlinear optical and optoelectronic properties, even for light at optical wavelengths. Such pronounced nonlinear optical effects have been studied in type-I Weyl semimetals, yet few studies have quantified these effects in type-II Weyl semimetals. We here present an optical experimental study with polarization resolution of two nonlinear optical effects in the type-II Weyl semimetal T_d -WTe₂. We begin by investigating the bulk optical second-harmonic response of this material using the rotational anisotropy of the second-harmonic generation. This technique allows us to simultaneously investigate the dependence of the second-harmonic response on the symmetry of the crystal and to quantify the size of that response, which we compare to other nonlinear crystals. We then use polarized time-resolved optical reflectivity spectroscopy to identify the nonlinear optical effect of impulsive stimulated Raman scattering as the origin of the coherent oscillations of the 0.25-THz shear mode. We find that the strength of this response in T_d -WTe₂ is enhanced compared with the observation of other modes excited through the dispersive excitation of coherent phonons. Notably, both the second-harmonic response and the coherent excitations of the phonons demonstrate strong anisotropy, displaying a clear dependence on the polarization of the light used in the experiments. We use point-symmetry analyses of the material to guide our understanding of these observations and perform fluence-dependent measurements to investigate the electron-phonon coupling.

DOI: [10.1103/PhysRevB.104.064304](https://doi.org/10.1103/PhysRevB.104.064304)

I. INTRODUCTION

Weyl semimetals (WSMs) are topological materials which exhibit a linear band dispersion near the Fermi energy described by the Weyl Hamiltonian of particle physics. The salient feature of the bulk dispersion is the crossing of the conduction and valence bands at topologically protected points, known as Weyl points (WPs). These WPs come in pairs of distinct and opposite chirality which serve as sources and sinks of Berry curvature. Quasiparticle excitations in these materials act as massless Weyl fermions. For this unique band structure to occur, either spatial inversion or time-reversal symmetry must be broken, resulting in electronic and magnetic WSMs, respectively [1,2]. Electronic WSMs which have mirror symmetries are typically classified as type I or type II, with type-II WSMs defined by a WP at the touching point of an electron and hole pocket [3]. Interest in WSMs has been robust because, in addition to their fundamental scientific interest, they have a wide breadth of potential applications, including broadband photodetection [4,5], new laser designs [6], and novel field-effect transistor devices with high on/off ratios and low power consumption [7].

The nonlinear optical properties of WSMs hold a particular interest. Multiple reports have shown anomalously strong nonlinear effects even at optical wavelengths, which is sometimes attributed to the topology of the band structure [8–10], and sometimes to more traditional electronic arguments. For example, WSMs are subject neither to screening by conduction electrons that lowers nonlinear responses in metals, nor to a band gap that lowers nonlinear responses in insulators and semiconductors [11]. Other studies have attributed anomalously large second-order responses to resonance effects [12]. One such nonlinear process, nonlinear photocurrent generation, has garnered much interest in WSMs both due to their large electron mobility and to their chiral response and the potential for quantization predicted by Weyl physics [13–18]. In addition, the large frequency doubling or second-harmonic generation (SHG) response observed in the type-I WSM TaAs [19,20] has been motivated by both topological and resonance effects [12,21]. While nonlinear effects including SHG [22], photocurrent generation [23], the nonlinear Hall effect [24], and higher-order effects [25] have all been observed in type-II WSMs, they are often studied in few- or monolayer materials rather than in bulk. Yet topological features like WPs and Weyl cones are bulk phenomena, motivating the study of nonlinear effects in bulklike thick type-II WSMs [26,27].

Here, we present an experimental study of two second-order nonlinear optical effects in the predicted type-II WSM, bulk T_d -WTe₂. First, we examine the SHG response and

*edruke@umich.edu

†lyzhao@umich.edu

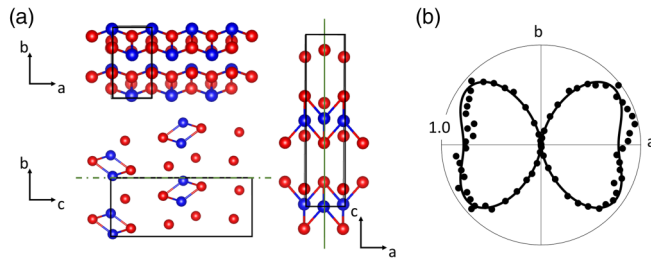


FIG. 1. (a) The crystal structure of T_d -WTe₂ drawn using VESTA software and crystallographic information from Refs. [29,30] along the a , b , and c axes. The mirror in the bc plane (solid green) and the glide mirror in the ac plane (dashed green) are indicated, and the unit cell is boxed in each orientation. (b) The RA-SHG data (dots) taken in the parallel channel and fit (solid curve) using the electric-dipole response of the m point group. The plot is normalized such that 1.0 corresponds to 32 fW.

estimate the size of the nonlinear optical susceptibility tensor, which we compare to other nonlinear crystals. Next, we use polarized time-resolved optical reflectivity spectroscopy to study the coherent oscillations of the optical phonons in this material. We identify the excitation mechanism of the lowest-frequency mode, the 0.25-THz shear mode, as the nonlinear process of impulsive stimulated Raman scattering (ISRS), distinct from other observed phonons excited through the dispersive excitation of coherent phonons (DECP). We find the strength of this nonlinear ISRS response to be large compared with the DECP response of the other modes. The 0.25-THz mode is further identified with an observation of the linear electro-optical effect. We use point-symmetry based analyses to study the anisotropic behavior of both the SHG and ISRS responses to the incoming light polarization. Finally, we use fluence-dependent measurements to verify our identified excitation mechanisms and to study the electron-phonon coupling.

II. CRYSTAL STRUCTURE AND SHG RESPONSE

The layered transition-metal dichalcogenide (TMDC) WTe₂ was the first predicted type-II WSM [3]. Like many layered TMDCs, it can exist in several different polytypes, including the T_d , $1T'$, and $2H$ phases. Of these, only the T_d phase is noncentrosymmetric and hosts the WSM state. However, unlike other layered TMDCs, WTe₂ exists in the T_d phase even at room temperature. The T_d phase is a distorted $1T'$ structure belonging to space group (point group) $Pmn2_1$ (C_{2v}) [28]. An illustration of the crystal structure of T_d -WTe₂ can be found in Fig. 1(a). It possesses a twofold screw axis along the c axis, a mirror in the bc plane, and a glide mirror in the ac plane.

Because T_d -WTe₂ is noncentrosymmetric, we in principle expect an electric-dipole SHG response. We can simultaneously confirm the symmetry of the sample and investigate its SHG response by measuring the rotational anisotropy of the SHG (RA-SHG) [31–33]. In most materials, the optical RA-SHG response is dictated by the point symmetries of the material obtained by eliminating translational symmetries of the space group because optical wavelengths are much longer than the lattice constants of the materials and therefore not

typically sensitive to translational symmetries. For the $Pmn2_1$ space group of T_d -WTe₂, this corresponding point group is C_{2v} . However, C_{2v} has mirrors in both the ac - and bc planes and therefore possesses an out-of-plane C_2 axis along the c axis which strictly forbids any SHG response at normal incidence. Figure 1(b) shows the reflected SHG intensity as a function of polarization angle when the incident fundamental and reflected SHG polarizations are parallel. Here, the fundamental light is incident normal to the ab plane of the crystal and its polarization is rotated in the plane [34]. In spite of the out-of-plane C_2 axis of C_{2v} , we see that there is a nonzero response in this experimental geometry, and that there is a large anisotropy in that response. This contradiction between our measurements and the point-group based prediction can be reconciled by the fact that T_d -WTe₂ possesses a glide mirror in the ac plane, or a mirror operation followed by a half unit-cell translation along the out-of-plane direction, or the incident light wave-vector direction. We find that the RA-SHG response of T_d -WTe₂ differentiates the glide plane from the mirror plane and thus demonstrates a nonzero SHG response even at normal incidence. We can then model the RA-SHG response using the symmetries of the m point group, which is a subgroup of $Pmn2_1$ containing only one mirror in the bc plane. The fit derived using the electric-dipole response of this point group for the parallel channel at normal incidence is shown in Fig. 1(b).

The signal strength of the RA-SHG measurements is used to estimate the strength of the SHG response. This is a crucial step towards understanding the strong nonlinear optical effects in type-II WSMs. To our knowledge, the refractive index of bulk T_d -WTe₂ has not been experimentally determined, but density-functional theory (DFT) calculations have recently been performed [35]. Using these calculated parameters to adjust for the nonlinear Fresnel coefficients [36], we find nonlinear susceptibility tensor elements of $\chi_{xyx} \approx 300$ pm/V, $\chi_{yxx} \approx 350$ pm/V, and $\chi_{yyy} \approx 200$ pm/V, which are each up to two orders of magnitude larger than previously reported measurements on nontopological polar metals [21,37,38]. Previous work on the SHG response of type-I WSMs revealed that the SHG response of TaAs (~ 7200 pm/V) was larger by an order of magnitude than that of GaAs at 800 nm (~ 600 pm/V) [21]. Our estimation for the SHG response in T_d -WTe₂ is about half that of GaAs.

There are several possible reasons for the discrepancy between the SHG responses for TaAs and T_d -WTe₂ observed here. One possible reason is that the polar axis of TaAs is the source of the strong SHG response in that material. While the c axis of T_d -WTe₂ is also a polar axis, we are not sensitive to it at normal incidence. The oblique incidence experimental geometry would allow us to access this polar axis, but the strength of the SHG response seems to be consistent between the normal and oblique incidence geometries, which are shown in Fig. S1 of Supplemental Material, Ref. [33]. Thus it seems unlikely that our experimental geometry is the source of the lower SHG response. The discrepancy might also come from the layered nature of the T_d -WTe₂ crystal structure, where $2d$ layers are only weakly connected via van der Waals interactions. This contrasts with the much stronger ionic bonding in TaAs along the polar axis. Yet another possible reason for the difference between the SHG response in

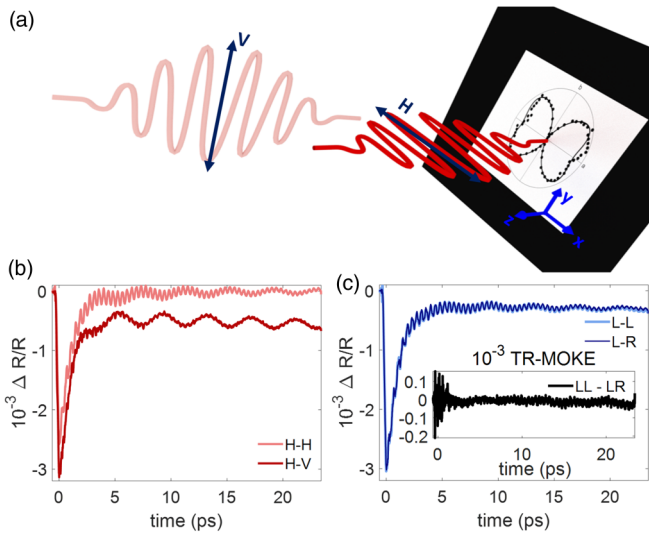


FIG. 2. (a) The experimental setup for the time-resolved reflectivity measurements. The pump pulse at 720 nm is normally incident on the sample and followed at a time delay by a probe pulse at 800 nm at a small oblique angle. The polarization of the pump and probe can be independently tuned into eight different polarization combinations and are shown here in the H - V channel. The lab frame is indicated in blue, and the sample coordinate system is indicated by the RA-SHG pattern. (b) Time-resolved reflectivity measurements for linearly polarized pump and probe in two polarization channels. In both channels, a dip in the change in reflectivity is observed at time zero followed by a decay with oscillations dependent on the polarization of the probe pulse. (c) Time-resolved reflectivity measurements for circularly polarized pump and probe. The inset illustrates the TR-MOKE signal calculated by subtracting the L - L and L - R polarization channels. A pump fluence of $\sim 127 \mu\text{J}/\text{cm}^2$ was used for data presented in (b) and (c).

TaAs and T_d -WTe₂ is that the wavelength of our fundamental light is farther from resonance than measurements taken on TaAs [12]. Indeed, optical conductivity measurements and DFT calculations on T_d -WTe₂ at room temperature indicate that the wavelengths used in this experiment are over two orders of magnitude removed from the band edge, and that the spectrum is otherwise smooth [35,39]. It is also possible that the difference between the SHG responses of T_d -WTe₂ and TaAs arises from the Weyl physics itself through carrier screening effects due to the presence of the electron and hole pockets at the WPs in T_d -WTe₂ which are not present in the type-I band structure. In metals, conduction electrons can screen the incoming fundamental field and thus reduce the second-harmonic response. In type-II WSMs, it is reasonable to expect that the presence of the electron and hole pockets near the WP might similarly provide carriers that would screen the incoming field and thus reduce the SHG response when compared with type-I WSMs. However, further study is needed to pin down the exact source of this discrepancy in the size of the SHG response between type-I and type-II WSMs.

III. TIME-RESOLVED REFLECTIVITY MEASUREMENTS

The experimental setup of the time-resolved optical reflectivity experiment is shown in Fig. 2(a). The pump is normal to

the sample surface and the probe is spatially separated from the reflected pump at the detector using a small oblique angle of incidence. The polarizations of the pump and probe pulses are independently tuned to yield eight polarization channels, labeled as pump polarization–probe polarization, consisting of combinations of left-hand circular polarization (L), right-hand circular polarization (R), linear horizontal polarization along the glide mirror direction with an uncertainty of $\pm 10^\circ$ (H), and linear vertical polarization along the mirror direction with an uncertainty of $\pm 10^\circ$ (V). All measurements are performed with a pump wavelength of 720 nm and a probe wavelength of 800 nm to allow pump discrimination with color filtering. The beam diameters of the pump and probe on the sample are ~ 50 and $\sim 30 \mu\text{m}$, respectively. The autocorrelation between the pump and probe is ~ 44 fs. The repetition rate is 200 kHz, and a chopper at 8 kHz is placed in the pump path to serve as a reference for a lock-in detector. Reflectivity measurements are taken using a silicon photodiode. Throughout, the probe fluence is about $65 \mu\text{J}/\text{cm}^2$.

The T_d -WTe₂ samples are synthesized using a self-flux method. WTe₂ powder of 0.2 g, and 10 g of Te (99.999%) are loaded into an alumina crucible, which is sealed in a quartz tube under vacuum. A small amount of quartz wool is later added on top of the alumina crucible to act as a filter in order to separate the flux from the crystals in a later step. The tube is then heated to 825 °C, held for 24 h, and then slowly cooled to 525 °C over 150 h. At 525 °C the flux is separated from the crystals by centrifuging. The WTe₂ crystals are then put in another vacuum-sealed quartz tube and annealed at 415 °C for 2 d. Prior to measurements, the sample is cleaved using Scotch tape in ambient conditions and immediately transferred to vacuum to prevent oxidation [40]. It is kept at room temperature in a vacuum better than 2×10^{-6} hPa.

Data using linearly polarized pump and probe are shown in Fig. 2(b). Although there is a clear distinction between the H - H and H - V polarization channels; the overall trend is defined by two key features. The first is the dramatic dip in the $\Delta R/R$ value at the temporal overlap point (time zero) of the pump and probe followed by a gradual recovery process. This dip is due to the excitation of electrons by the pump pulse. The recovery following the dip can be fit using two exponential decays convolved with a Gaussian beam profile. We find one shorter time constant on the order of 1 ps, which we associate with electron-phonon thermalization, and a longer weak decay on the order of 5–10 ps previously associated with phonon-assisted electron-hole recombination [41]. The second feature is the oscillatory behavior in the dynamic response after time-zero, which we associate with coherent excitations of optical phonons. The frequencies of these oscillations are extracted by subtracting the fit for the relaxation dynamics and performing a fast Fourier transform (FFT). Throughout all channels, six phonon oscillations are observed at 0.25, 2.4, 3.5, 3.9, 4.9, and 6.4 THz [Fig. 3(b)]. All observed phonons are associated with A_1 modes by comparing their frequencies to previous Raman measurements [40,42–45]. An example of the fit to the relaxation dynamics and the extracted oscillations are shown for the L - L channel in Fig. 3(a).

Figure 2(c) shows time-resolved reflectivity measurements for circularly polarized pump and probe beams. The same

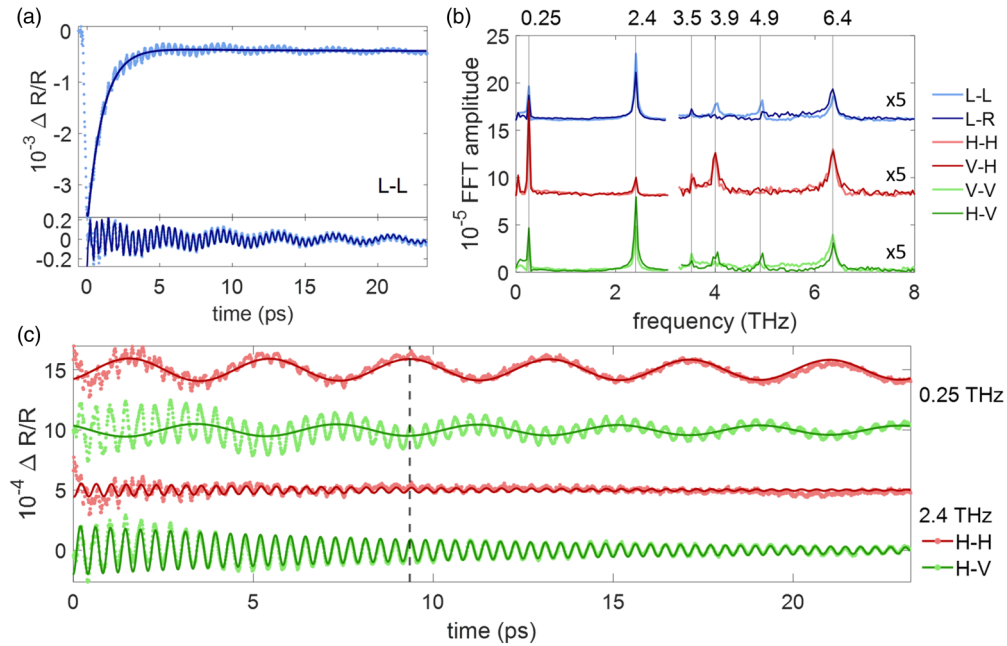


FIG. 3. (a) An illustration of the fitting procedure used in the data analysis in the case of an L - L dataset. First, the decay dynamics are fit to the sum of two exponential decays convolved with a Gaussian beam. This fit is then subtracted from the data to reveal the underlying phonon oscillations, which are fit individually assuming decaying sinusoidal oscillations. (b) The FFT of the raw phonon oscillations for various polarization channels, with the spectrum above 3 THz enhanced by a factor of 5 for clarity. There is a clear dependence of the strength of the observed phonons on the probe polarization. (c) An illustration of the oscillations at 0.25 and 2.4 THz for the H - H and H - V channels. Using the dashed line as a guide, a phase difference of π between these two channels can be observed for 0.25 THz which is not present in the oscillations at 2.4 THz. This is indicative of the linear electro-optical effect.

relaxation and oscillatory features can be seen in these data as were observed in the linear polarization channels, although the phonon oscillations exhibit significantly less distinction between channels. The inset of Fig. 2(c) demonstrates a null result for a time-resolved magneto-optical Kerr effect (TR-MOKE) signal under our experimental conditions, calculated by subtracting the L - L and L - R channels, in spite of the expectation of such a signal in WSMs due to the chirality of the Weyl cones. This is likely because the pump wavelength will excite electrons far above the chiral WPs to higher bands whose response will dominate over that expected using topological arguments.

Figures 2(b) and 2(c) demonstrate that the oscillations of the phonon modes depend on the polarization channel, and Figs. 3(b) and 3(c) show this dependence quantitatively by demonstrating the polarization dependence of the phonon amplitudes and phases, respectively. In Fig. 3(b), the FFTs of the oscillations of the data are shown for the L - L , L - R , H - H , V - H , H - V , and V - V channels (data for additional polarization channels are available [33]). Immediately it is clear that there is a strong anisotropy in the coherently excited phonons, as the amplitudes of the oscillations depend on the polarization of the probe beam for the linear channels. For example, the 2.4-THz mode is preferentially sampled with vertically polarized probe while the 3.9-THz mode is preferentially sampled with horizontally polarized probe. In Fig. 3(c), the oscillations of the two strongest phonons at 0.25 and 2.4 THz are highlighted. We observe that the 0.25-THz mode oscillates sinusoidally and has a phase of π between H and V polarized

probe while the 2.4-THz mode oscillates cosinusoidally in all linear polarization channels.

First, we will discuss what these dependencies tell us about the excitation mechanism of the coherent phonons. The origin of the excitations of the coherent phonons is typically assigned to either DECP or ISRS. In DECP, the coherent excitation is driven by the perturbation of the pump beam to the electronic distribution and is dictated by the potential landscape of the phonons [46]. ISRS, in contrast, is a nonlinear optical effect where excitations occur due to mixing within the pump beam at frequencies accessible through difference frequency generation of the broad pulse spectrum [47]. Important differences exist in the phonons excited by these two mechanisms. For example, in DECP, only fully symmetric A_1 Raman modes can be excited with a $\cos(\omega t)$ dependence, while ISRS can excite modes of any symmetry and will only exhibit a $\cos(\omega t)$ dependence when the incoming light is at resonance excitations. We fit the oscillations in the data to a decaying sine curve, as

$$f(t) = ae^{-t/\tau} \sin(\omega t + \phi), \quad (1)$$

and find the extracted phase of the 2.4-THz mode to be 4.524 ± 0.13 ($260^\circ \approx 1.45\pi$) for the H - H channel and 4.880 ± 0.025 ($280^\circ \approx 1.55\pi$) for the H - V channel, as shown in Fig. 3(c). Because our pump laser is far from resonance and the 2.4-THz mode has a $\cos(\omega t)$ dependence, as shown in Fig. 3(c), we can identify its excitation mechanism as DECP. In contrast, the extracted phases of the 0.25-THz mode are found to be 5.338 ± 0.05 ($305^\circ \approx 1.67\pi$) for the H - H channel and 2.373 ± 0.189 ($136^\circ \approx 0.76\pi$) for the H - V channel.

That is, $\sim 50^\circ$ off from a pure sine or pure cosine in either channel. However, the deviation from a pure cosine dependence indicates the presence of some ISRS response of this mode [46,48–53]. The oscillations of the remaining phonons are too weak to be directly visualized in this way, and fitting them to exponentially decaying sinusoidal functions leads to large uncertainties. However, past experiments have also assigned them to DECP [54,55].

The strength of the ISRS excitation relative to the DECP excitations is worthy of note. The first predictions and observations of DECP suggested that these oscillations would be very large, especially compared with ISRS excitations [46,49]. And indeed, in materials in which both excitation mechanisms are observed simultaneously, the ISRS excitations have been significantly weaker [56]. Theory predictions suggest that DECP and ISRS arise from the real and imaginary components of the same tensor, with ISRS dominating in regimes near an absorption edge or an impurity feature [48]. Yet DFT calculations on T_d -WTe₂ suggest that we are not in this special regime [35]. This implies that, from our polarization-resolved data alone, we may not pin down the precise reason for the dominance of the ISRS mechanism in the case of the shear mode excitation. Thus, to gain a better perspective on the phonon excitation mechanisms, we will investigate the fluence dependence of the time constant dictated by electron-phonon interactions below.

There are two subtleties in our identified excitation mechanisms. First, because all of the modes but the 0.25-THz mode are associated with DECP, they must all be A_1 . Yet they do not all have the same polarization dependence, as illustrated in Fig. 3(b). Second, the pump-polarization dependence typical of ISRS is not found in our measurements. Both of these phenomena can be explained by investigating the polarization of the light incident on the sample in the framework of the C_{2v} symmetry of the material. In particular, because the experimental linear polarizations of the pump and probe beams are aligned to the high-symmetry axes of the crystal, V and H can be represented as the B_1 and B_2 irreducible representations (irreps) of the C_{2v} point group, respectively. We can then consider the selection rules for ISRS, which arise due to the mixing of two identical copies of the pump pulse. In C_{2v} , the direct product of any irrep with itself will lead to A_1 symmetry. Thus, the polarization response will be entirely dependent on the symmetry of the probe. Further, by looking at the form of the A_1 irrep for C_{2v} , which is given by

$$A_1 = \begin{pmatrix} a & 0 & 0 \\ 0 & b & 0 \\ 0 & 0 & c \end{pmatrix}, \quad (2)$$

we can see that it is possible for opposite probe-polarization dependencies to result from two A_1 modes depending on the strength of the a and b elements for each mode [33,45,57].

In addition to the excitation mechanism, an analysis of the phase of the 0.25-THz mode reveals the appearance of the linear electro-optical effect through a phase shift between the H and V probe channels as shown in Fig. 3(c). This phase shift was first reported in time-resolved optical reflectivity measurements on GaAs [50]. Because C_{2v} is an anisotropic point group, the pump will cause inequivalent changes to the indices of refraction along the a and b crystal axes which are

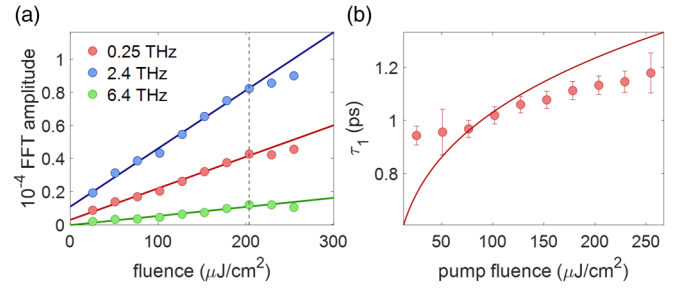


FIG. 4. (a) Fluence dependence of the FFT amplitudes of the three strongest coherently excited phonons, indicating that all measurements were taken in the linear regime. The solid lines guide the eye for a linear fit to the data. A kink in this linear behavior can be seen for all three oscillations after $200 \mu\text{J}/\text{cm}^2$, indicated by the dashed line. (b) The fluence dependence of time constant τ_1 dictating the electron-phonon thermalization time with a TTM fit.

then sampled by the probe. This can also be understood from a symmetry perspective. In particular, the 0.25-THz mode is known to be a shear mode, an optical phonon mode characterized by intra-unit-cell motion along the glide mirror axis which has been shown to induce a phase transition from the T_d phase to the $1T'$ phase [27]. A more detailed calculation of this effect is shown in Refs. [33,58].

To further motivate the nonlinear ISRS excitation of the 0.25-THz shear mode, we investigated the pump fluence dependence of the phonon amplitudes, shown in Fig. 4(a). We expect this dependence to be linear because ISRS is reliant on the mixing of two copies of the electric field of the pump at frequencies ω and $\omega + \Omega$ to excite a phonon of frequency Ω . Indeed, we find that the phonon amplitude is linearly dependent on this pump fluence. The amplitudes of the two strongest DECP excitations at 2.4 and 6.4 THz are also shown in Fig. 4(a) to be linearly dependent on the pump fluence, but in the case of DECP this is because there is a larger number of excited carriers at higher fluences rather than because of nonlinear mixing of the fields. Interestingly, it seems there is a divergence from the otherwise linear dependence of all three modes after $200 \mu\text{J}/\text{cm}^2$. In similar measurements on the related material MoTe₂, such a divergence was indicative of a light-induced change in the lattice symmetry [26]. There is also the possibility of a nonzero intercept for the 2.4-THz mode, but this is likely caused by the sensitivity of the experiment or due to a larger probe fluence for measurements taken at the smallest pump fluences.

To gather more information on the mechanism behind the large ISRS excitation of the 0.25-THz mode, we also investigated the electron-phonon thermalization time, shown in Fig. 4(b), which is directly related to the electron-phonon coupling constant. This time constant has previously been analyzed for increasing lattice temperature [41]. We performed a two-temperature model (TTM) fit to our data [59–62], assuming a purely thermal effect and using material parameters derived using DFT calculations [35]. In particular, we model the electron-phonon thermalization time as

$$\tau_{e-ph} = \frac{\gamma(T_e^2 - T_l^2)}{2H(T_e, T_l)}, \quad (3)$$

where T_e is the electron temperature, T_l is the lattice temperature, γ is the electron specific heat-coefficient, used as a fitting parameter, and

$$H(T_e, T_l) = f(T_e) - f(T_l) \quad (4)$$

for

$$f(T) = 4g_\infty \frac{T^5}{\Theta_D^4} \int_0^{\frac{\Theta_D}{T}} \frac{x^4}{e^x - 1} dx, \quad (5)$$

for Θ_D the Debye temperature, taken to be 133.8 K [41], and g_∞ the electron-phonon coupling constant, which is the second fitting parameter used in our model. T_e is computed as

$$T_e = \left(T_l^2 + \frac{2U_l}{\gamma} \right)^{1/2}, \quad (6)$$

for U_l the deposited laser energy density. T_l is taken to be 293 K because all measurements were taken at room temperature. However, an adjustment to T_l is made to account for laser heating. In particular, we take

$$T_{l,f} = \left(\frac{E_{\text{laser}}}{C} + T_{l,i}^4 \right)^{1/4}, \quad (7)$$

for E_{laser} the energy deposited in the material per pulse, C a constant equal to 1.658×10^{-16} , and $T_{l,f}$ and $T_{l,i}$ the final and initial lattice temperature values, respectively [62]. This method yields $\gamma \approx 10.2 \text{ mJ mol}^{-1} \text{ K}^{-2}$ and $g_\infty \approx 6.79 \times 10^{15} \text{ W m}^{-3} \text{ K}^{-1}$. While the TTM fit matches the monotonic trend of the data, it was not found to fit the data well, in contrast with previous experiments [41]. This may be because the fluence used here is two orders of magnitude larger than that used in previous measurements, and the TTM assumption of a purely thermal response between the lattice and excited electrons breaks down as we move away from the perturbative regime, especially because the 720-nm pump excites well above the Fermi energy. Because our fluence-dependent measurements of the FFT amplitude of the phonon modes indicate that we are in the linear regime [46,63], and because we are well below the previously reported damaged threshold [25], there may be an additional mechanism involved in reaching equilibrium between the electrons and phonons after excitation. One such possibility is interactions between the phonons and Weyl fermion excitations, which has previously been reported in TaAs [64]. Such an interaction might be indicated by the asymmetric line shape of the 0.25-THz mode observed in the FFT spectrum [33].

IV. CONCLUSION

We present an analysis of the strength and anisotropy of the nonlinear optical processes of SHG and ISRS in the bulk type-II WSM $T_d\text{-WTe}_2$. We identify a large SHG response relative to nontopological polar metals, but one which is smaller than that reported previously for type-I WSMs. We find that this SHG response has a strong anisotropy dependent on the polarizations of the incoming fundamental and reflected frequency-doubled light. We also observe ISRS through the oscillations of the 0.25-THz interlayer shear mode which is at least as large as the DECP response, in contrast to previous measurements in which both excitation mechanisms are observed concurrently within a material where the DECP response dominates over the ISRS response, and despite our experimental parameters keeping the excitations away from resonance in the DFT calculated band structure. This ISRS excitation is also strongly anisotropic, with an amplitude depending on the incoming probe polarization. This mode also demonstrates the linear electro-optical effect.

Previous studies have linked the 0.25-THz shear mode to Weyl physics in $T_d\text{-WTe}_2$ [55]. This, coupled with the insufficiency of the TTM to fit the fluence dependence of the electron-phonon time constant, suggests interactions between this mode and Weyl fermion excitations might play a role in the relaxation dynamics [33]. In addition, previous observations of the electro-optical effect have been associated with surface field enhancements of phonon excitations [50–53,65,66]. The observation of this effect through the shear mode suggests the potential for enhancing the shear mode response with the application of some in-plane electric field, either by applying a bias or inducing a photocurrent [23], which might further enhance the nonlinear effects in this material.

The data that support the findings of this study are available from the corresponding author upon reasonable request.

ACKNOWLEDGMENTS

E.D. acknowledges support by the NSF Graduate Research Fellowship Program under Grant No. DGE 1841052, as well as support from Delta Solutions and Strategies, LLC. L.Z. acknowledges support from NSF CAREER Grant No. DMR-174774.

J.Y. fabricated the samples. E.D. performed all experiments and data analysis, and E.D. and L.Z. wrote the text.

-
- [1] A. A. Burkov, *Nat. Mater.* **15**, 1145 (2016).
 [2] S. A. Yang, *SPIN* **06**, 1640003 (2016).
 [3] A. A. Soluyanov, D. Gresch, Z. Wang, Q. Wu, M. Troyer, X. Dai, and B. A. Bernevig, *Nature (London)* **527**, 495 (2015).
 [4] S. Chen, L. Miao, X. Chen, Y. Chen, C. Zhao, S. Datta, Y. Li, Q. Bao, H. Zhang, Y. Liu, S. Wen, and D. Fan, *Adv. Opt. Mater.* **3**, 1769 (2015).
 [5] S. Chi, Z. Li, Y. Xie, Y. Zhao, Z. Wang, L. Li, H. Yu, G. Wang, H. Weng, H. Zhang, and J. Wang, *Adv. Mater.* **30**, 1801372 (2018).
 [6] G. Oktay, M. Sarisaman, and M. Tas, *Sci. Rep.* **10**, 3127 (2020).
 [7] G. Chen, W. Chen, and O. Zilberberg, *APL Mater.* **8**, 011102 (2020).
 [8] T. Morimoto and N. Nagaosa, *Sci. Adv.* **2**, e1501524 (2016).
 [9] D. Hsieh, J. W. McIver, D. H. Torchinsky, D. R. Gardner, Y. S. Lee, and N. Gedik, *Phys. Rev. Lett.* **106**, 057401 (2011).
 [10] D. Smirnova, D. Leykam, Y. Chong, and Y. Kivshar, *Appl. Phys. Rev.* **7**, 021306 (2020).

- [11] N. Nagaosa, T. Morimoto, and Y. Tokura, *Nat. Rev. Mater.* **5**, 621 (2020).
- [12] S. Patankar, L. Wu, B. Lu, M. Rai, J. D. Tran, T. Morimoto, D. E. Parker, A. G. Grushin, N. L. Nair, J. G. Analytis, J. E. Moore, J. Orenstein, and D. H. Torchinsky, *Phys. Rev. B* **98**, 165113 (2018).
- [13] G. B. Osterhoudt, L. K. Diebel, M. J. Gray, X. Yang, J. Stanco, X. Huang, B. Shen, N. Ni, P. J. W. Moll, Y. Ran, and K. S. Burch, *Nat. Mater.* **18**, 471 (2019).
- [14] D. Rees, K. Manna, B. Lu, T. Morimoto, H. Borrmann, C. Felser, J. E. Moore, D. H. Torchinsky, and J. Orenstein, *Sci. Adv.* **6**, eaba0509 (2020).
- [15] C.-K. Chan, N. H. Lindner, G. Refael, and P. A. Lee, *Phys. Rev. B* **95**, 041104(R) (2017).
- [16] G. Chang, J.-X. Yin, T. Neupert, D. S. Sanchez, I. Belopolski, S. S. Zhang, T. A. Cochran, Z. Chéng, M.-C. Hsu, S.-M. Huang, B. Lian, S.-Y. Xu, H. Lin, and M. Z. Hasan, *Phys. Rev. Lett.* **124**, 166404 (2020).
- [17] F. de Juan, A. G. Grushin, T. Morimoto, and J. E. Moore, *Nat. Commun.* **8**, 15995 (2017).
- [18] N. Sirica, R. I. Tobey, L. X. Zhao, G. F. Chen, B. Xu, R. Yang, B. Shen, D. A. Yarotski, P. Bowlan, S. A. Trugman, J. X. Zhu, Y. M. Dai, A. K. Azad, N. Ni, X. G. Qiu, A. J. Taylor, and R. P. Prasankumar, *Phys. Rev. Lett.* **122**, 197401 (2019).
- [19] B. Q. Lv, H. M. Weng, B. B. Fu, X. P. Wang, H. Miao, J. Ma, P. Richard, X. C. Huang, L. X. Zhao, G. F. Chen, Z. Fang, X. Dai, T. Qian, and H. Ding, *Phys. Rev. X* **5**, 031013 (2015).
- [20] S.-Y. Xu, I. Belopolski, N. Alidoust, M. Neupane, G. Bian, C. Zhang, R. Sankar, G. Chang, Z. Yuan, C.-C. Lee, S.-M. Huang, H. Zheng, J. Ma, D. S. Sanchez, B. Wang, A. Bansil, F. Chou, P. P. Shibayev, H. Lin, S. Jia, and M. Z. Hasan, *Science* **349**, 613 (2015).
- [21] L. Wu, S. Patankar, T. Morimoto, N. L. Nair, E. Thewalt, A. Little, J. G. Analytis, J. E. Moore, and J. Orenstein, *Nat. Phys.* **13**, 350 (2016).
- [22] Y. Chen, B. Peng, C. Cong, J. Shang, L. Wu, W. Yang, J. Zhou, P. Yu, H. Zhang, Y. Wang, C. Zou, J. Zhang, S. Liu, Q. Xiong, H. Shao, Z. Liu, H. Zhang, W. Huang, and T. Yu, *Adv. Mater.* **31**, 1804979 (2019).
- [23] M. Chen, K. Lee, J. Li, L. Cheng, Q. Wang, K. Cai, E. E. M. Chia, H. Chang, and H. Yang, *ACS Nano* **14**, 3539 (2020).
- [24] I. Sodemann and L. Fu, *Phys. Rev. Lett.* **115**, 216806 (2015).
- [25] M. He, Y. Chen, L. Zhu, H. Wang, X. Wang, X. Xu, and Z. Ren, *Photon. Res.* **7**, 1493 (2019).
- [26] M. Y. Zhang, Z. X. Wang, Y. N. Li, L. Y. Shi, D. Wu, T. Lin, S. J. Zhang, Y. Q. Liu, Q. M. Liu, J. Wang, T. Dong, and N. L. Wang, *Phys. Rev. X* **9**, 021036 (2019).
- [27] E. J. Sie, C. M. Nyby, C. D. Pemmaraju, S. J. Park, X. Shen, J. Yang, M. C. Hoffmann, B. K. Ofori-Okai, R. Li, A. H. Reid, S. Weathersby, E. Mannebach, N. Finney, D. Rhodes, D. Chenet, A. Antony, L. Balicas, J. Hone, T. P. Devereaux, T. F. Heinz, X. Wang, and A. M. Lindenberg, *Nature (London)* **565**, 61 (2019).
- [28] S.-Y. Xu, Q. Ma, H. Shen, V. Fatemi, S. Wu, T.-R. Chang, G. Chang, A. M. M. Valdivia, C.-K. Chan, Q. D. Gibson, J. Zhou, Z. Liu, K. Watanabe, T. Taniguchi, H. Lin, R. J. Cava, L. Fu, N. Gedik, and P. Jarillo-Herrero, *Nat. Phys.* **14**, 900 (2018).
- [29] P. Villars, PAULING FILE, in *Inorganic Solid Phases*, SpringerMaterials (online database), Springer, Heidelberg (ed.) SpringerMaterials.
- [30] VESTA license, <https://jp-minerals.org/vesta/en/download.html>; K. Momma and F. Izumi, *J. Appl. Crystallogr.* **44**, 1272 (2011).
- [31] D. H. Torchinsky, H. Chu, T. Qi, G. Cao, and D. Hsieh, *Rev. Sci. Instrum.* **85**, 083102 (2014).
- [32] J. W. Harter, L. Niu, A. J. Woss, and D. Hsieh, *Opt. Lett.* **40**, 4671 (2015).
- [33] See Supplemental Material at <http://link.aps.org/supplemental/10.1103/PhysRevB.104.064304> for more detailed information on the RA-SHG experimental setup and modeling, the symmetry analysis of the excited phonon modes, and a mathematical description of the Pockels effect. All files related to a published paper are stored as a single deposit and assigned a Supplemental Material URL. This URL appears in the article's reference list.
- [34] W. Jin, E. Druke, S. Li, A. Admasu, R. Owen, M. Day, K. Sun, S.-W. Cheong, and L. Zhao, *Nat. Phys.* **16**, 42 (2020).
- [35] B. Rahman Rano, I. M. Syed, and S. H. Naqib, *Results Phys.* **19**, 103639 (2020).
- [36] N. Bloembergen and P. S. Pershan, *Phys. Rev.* **128**, 606 (1962).
- [37] H. Padmanabhan, Y. Park, D. Puggioni, Y. Yuan, Y. Cao, L. Gasparov, Y. Shi, J. Chakhalian, J. M. Rondinelli, and V. Gopalan, *Appl. Phys. Lett.* **113**, 122906 (2018).
- [38] K. Markey, T. Putzeys, P. Horcajada, T. Devic, N. Guillou, M. Wübbenhorst, S. V. Cleuvenbergen, T. Verbiest, D. E. De Vos, and M. A. van der Veen, *Dalton Trans.* **45**, 4401 (2016).
- [39] C. C. Homes, M. N. Ali, and R. J. Cava, *Phys. Rev. B* **92**, 161109(R) (2015).
- [40] C.-H. Lee, E. C. Silva, L. Calderin, M. A. T. Nguyen, M. J. Hollander, B. Bersch, T. E. Mallouk, and J. A. Robinson, *Sci. Rep.* **5**, 10013 (2015).
- [41] Y. M. Dai, J. Bowlan, H. Li, H. Miao, S. F. Wu, W. D. Kong, P. Richard, Y. G. Shi, S. A. Trugman, J. X. Zhu, H. Ding, A. J. Taylor, D. A. Yarotski, and R. P. Prasankumar, *Phys. Rev. B* **92**, 161104(R) (2015).
- [42] W. D. Kong, S. F. Wu, P. Richard, C. S. Lian, J. T. Wang, C. L. Yang, Y. G. Shi, and H. Ding, *Appl. Phys. Lett.* **106**, 081906 (2015).
- [43] M. K. Jana, A. Singh, D. J. Late, C. R. Rajamathi, K. Biswas, C. Felser, U. V. Waghmare, and C. N. R. Rao, *J. Phys: Condens. Matter* **27**, 285401 (2015).
- [44] Y. C. Jiang, J. Gao, and L. Wang, *Sci. Rep.* **6**, 19624 (2016).
- [45] Q. Song, X. Pan, H. Wang, K. Zhang, Q. Tan, P. Li, Y. Wan, Y. Wang, X. Xu, M. Lin, X. Wan, F. Song, and L. Dai, *Sci. Rep.* **6**, 29254 (2016).
- [46] H. J. Zeiger, J. Vidal, T. K. Cheng, E. P. Ippen, G. Dresselhaus, and M. S. Dresselhaus, *Phys. Rev. B* **45**, 768 (1992).
- [47] Y. X. Yan, E. B. Gamble, and K. A. Nelson, *J. Chem. Phys.* **83**, 5391 (1985).
- [48] T. E. Stevens, J. Kuhl, and R. Merlin, *Phys. Rev. B* **65**, 144304 (2002).
- [49] T. K. Cheng, J. Vidal, H. J. Zeiger, G. Dresselhaus, M. S. Dresselhaus, and E. P. Ippen, *Appl. Phys. Lett.* **59**, 1923 (1991).
- [50] G. C. Cho, W. Kütt, and H. Kurz, *Phys. Rev. Lett.* **65**, 764 (1990).
- [51] T. Dekorsy, T. Pfeifer, W. Kütt, and H. Kurz, *Phys. Rev. B* **47**, 3842 (1993).
- [52] W. A. Kutt, W. Albrecht, and H. Kurz, *IEEE J. Quantum Electron.* **28**, 2434 (1992).
- [53] T. Pfeifer, T. Dekorsy, W. Kütt, and H. Kurz, *Appl. Phys. A* **55**, 482 (1992).

- [54] T. Fukuda, K. Makino, Y. Saito, P. Fons, A. V. Kolobov, K. Ueno, and M. Hase, *Appl. Phys. Lett.* **116**, 093103 (2020).
- [55] P. Hein, S. Jauernik, H. Erk, L. Yang, Y. Qi, Y. Sun, C. Felser, and M. Bauer, *Nat. Commun.* **11**, 2613 (2020).
- [56] A. Q. Wu and X. Xu, *Appl. Surf. Sci.* **253**, 6301 (2007).
- [57] R. A. Bartels, S. Backus, M. M. Murnane, and H. C. Kapteyn, in *Conference on Lasers and Electro-Optics/Quantum Electronics and Laser Science Conference*, Technical Digest (Optical Society of America, 2003), paper QThJ17.
- [58] J. W. McIver, D. Hsieh, S. G. Drapcho, D. H. Torchinsky, D. R. Gardner, Y. S. Lee, and N. Gedik, *Phys. Rev. B* **86**, 035327 (2012).
- [59] P. B. Allen, *Phys. Rev. Lett.* **59**, 1460 (1987).
- [60] L. Cheng, C. La-o-vorakiat, C. S. Tang, S. K. Nair, B. Xia, L. Wang, J.-X. Zhu, and E. E. M. Chia, *Appl. Phys. Lett.* **104**, 211906 (2014).
- [61] R. H. M. Groeneveld, R. Sprik, and A. Lagendijk, *Phys. Rev. B* **51**, 11433 (1995).
- [62] A. Slachter, Time resolved Kerr rotation and reflectance on 2D and 1D confined electron spins in an AlGaAs/GaAs heterojunction, Master thesis, University of Groningen, 2006.
- [63] J. Lee, J. R. Challa, and D. W. McCamant, *J. Raman Spectrosc.* **44**, 1263 (2013).
- [64] B. Xu, Y. M. Dai, L. X. Zhao, K. Wang, R. Yang, W. Zhang, J. Y. Liu, H. Xiao, G. F. Chen, S. A. Trugman, J. X. Zhu, A. J. Taylor, D. A. Yarotski, R. P. Prasankumar, and X. G. Qiu, *Nat. Commun.* **8**, 14933 (2017).
- [65] J. P. Heritage, J. G. Bergman, A. Pinczuk, and J. M. Worlock, *Chem. Phys. Lett.* **67**, 229 (1979).
- [66] G. A. Garrett, T. F. Albrecht, J. F. Whitaker, and R. Merlin, *Phys. Rev. Lett.* **77**, 3661 (1996).